Title

Spatial Organization and Molecular Interactions of the Schizosaccharomyces pombe Ccq1—Tpz1—Poz1 Shelterin Complex

Journal

Journal of Molecular Biology, 429(19)

ISSN

0022-2836

Authors

Scott, Harry
Kim, Jin-Kwang
Yu, Clinton
et al.

Publication Date

2017-09-01

DOI

10.1016/j.jmb.2017.08.002

Peer reviewed

Published in final edited form as:

J Mol Biol. 2017 September 15; 429(19): 2863–2872. doi:10.1016/j.jmb.2017.08.002.

Spatial organization and molecular interactions of the *Schizosaccharomyces pombe* Ccq1-Tpz1-Poz1 shelterin complex

Harry Scott[1,†], **Jin-Kwang Kim**[3,†], **Clinton Yu**[4], **Lan Huang**[4], **Feng Qiao**[3,5], and **Derek J. Taylor**[1,2,5]

[1]Department of Pharmacology, Case Western Reserve University, Cleveland OH 44106

[2]Department of Biochemistry, Case Western Reserve University, Cleveland OH 44106

[3]Department of Biological Chemistry, University of California Irvine, Irvine CA 92697

[4]Department of Physiology and Biophysics, University of California Irvine, Irvine CA 92697

Abstract

The shelterin complex is a macromolecular assembly of proteins that binds to and protects telomeric DNA, which composes the ends of all linear chromosomes. Shelterin proteins prevent chromosome ends from fusing together and from eliciting erroneous induction of DNA damage response pathways. Additionally, shelterin proteins play key roles in regulating the recruitment and activation of telomerase, an enzyme that extends telomeric DNA. In fission yeast, *Schizosaccharomyces pombe*, interactions between the shelterin proteins Ccq1, Tpz1, and Poz1, are important for regulating telomerase-mediated telomere synthesis, and thus, telomere length homeostasis. Here, we used electron microscopy combined with genetic labeling to define the three-dimensional arrangement of the *S. pombe* Ccq1-Tpz1-Poz1 (CTP) complex. Cross-linking mass spectrometry was used to identify individual residues that are in proximity to the protein-protein interfaces of the assembled CTP complex. Together, our data provide a first glimpse into the architectural design of the CTP complex and reveals unique interactions that are important in maintaining the *S. pombe* telomere in a non-extendible state.

Graphical Abstract

[5]Correspondence to: derek.taylor@case.edu; qiao@uci.edu.
[†]These authors contributed equally to this work

Accession Numbers

The electron density maps for C_fTP, $_mC_fTP$, C_fT_mP, and C_nTP have been deposited into the EMDataBank with accession numbers EMD-8863, EMD-8864, EMD-8865 and EMD-8866, respectively.

Author Contributions

H.S., F.Q., and D.J.T. designed the study. J-K.K. expressed and purified all proteins, including those with the MBP tags, and performed protein cross-linking and biochemical analyses of assembled complexes. H.S. collected EM data and determined the structures. C.Y. and L.H. performed cross-linking mass spectrometry experiments and data analysis. H.S., J-K.K., F.Q. and D.J.T. analyzed the data. H.S., F.Q. and D.J.T. wrote the paper. All authors discussed the results and interpretations throughout the experimental procedures and during manuscript preparation.

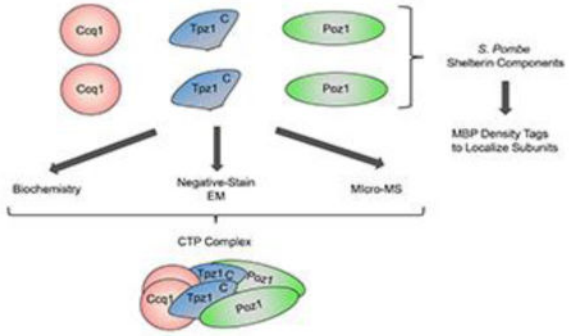

Keywords

Telomere; telomerase; extension; protection; electron microscopy

Telomeres are nucleoprotein complexes that cap the ends of eukaryotic chromosomes [1]. The DNA component of telomeres consists of repetitive G-rich sequences that extend for thousands of bases of double-stranded (ds) DNA before ending in short, single-stranded (ss) DNA overhangs [1,2]. Because DNA polymerases are unable to synthesize the extreme end of the lagging strand, linear chromosomes become progressively shorter after each round of DNA replication and cell division [3]. Thus, one function of the repetitive telomeric DNA is to absorb this shortening event without incurring the loss of genetic information [4]. In both mammalian somatic cells and single-celled eukaryotes (such as yeast) with genetically inactivated telomerase, continuous telomere erosion upon cell propagations results in critically short telomeres, making genomic DNA more susceptible to alterations and chromosome ends more prone to end-to-end fusions [5–7]. To avoid this catastrophic event, cells initiate replicative senescence to halt cell division when telomeres reach a critically short length [8]. Conversely, cells that propagate indefinitely, such as human embryonic stem cells, the majority of cancer cells, and wild-type single-celled eukaryotes including ciliated protozoa and yeasts, avoid replicative senescence by sustaining elevated levels of telomerase activity [9,10]. Telomerase is a specialized ribonucleoprotein (RNP) enzyme with reverse transcriptase activity and an intrinsic long noncoding RNA molecule that serves as a template to extend the telomeric DNA [11]. Telomere extension by telomerase allows for continuous proliferation of these cells, as it serves to protect against telomere attrition and thus the deleterious effects triggered by extremely short telomeres. In fission yeast, *Schizosaccharomyces pombe*, telomerase-mediated telomere elongation functions to maintain telomere length homeostasis throughout successive cell divisions [12].

A specialized multi-protein complex called shelterin binds to the telomeric DNA to protect it from eliciting aberrant DNA damage signaling and for regulating telomerase activity [1,5,7,13]. The shelterin complex is well conserved, particularly between mammals and fission yeast, and consists of proteins that recognize both ds and ss telomere DNA specifically (Fig. S1). In the mammalian complex, TIN2 and ACD (previously known as TPP1) form a protein linker connecting ss and dsDNA-binding proteins, an action that is important for regulating telomere length [14,15]. In *S. pombe*, shelterin components Ccq1,

Tpz1 (ACD ortholog), and Poz1 (TIN2 ortholog) form a similar sub-complex (CTP complex) that fills this role [16].

In addition to contributing to telomere length homeostasis, the protein-protein interactions of the *S. Pombe* CTP complex are known to regulate other cellular processes as well (Fig. 1a). For example, Ccq1 mediates the physical interaction between the shelterin complex and the histone H3K9 methyltransferase Clr4 complex (CLRC) to establish telomeric heterochromatin [17]. The CTP complex interactions, which are coordinated by the Tpz1 C-terminal domain (CTD) [18,19] (Fig. 1b), are additionally important for regulating telomere protection versus telomerase-mediated telomere extension. The Ccq1-Tpz1 interaction promotes telomere extension by controlling telomere switching from a non-extendible to an extendible state and by participating in the cell-cycle regulated telomerase recruitment [20,21]. Recruitment of telomerase is mediated through Ccq1-Est1 interactions coupled with Tpz1-Trt1 (catalytic subunit of telomerase) interactions that are initiated by phosphorylation of Ccq1 [20–23] (Fig. 1a). In contrast, mutants that disrupt the Tpz1-Poz1 interaction of the CTP complex result in uncontrolled telomerase-mediated telomere extension [16]. Together, these data indicate that the CTP sub-complex exhibits both positive and negative regulatory roles in telomerase-mediated telomere elongation.

Currently, published structural information regarding the CTP complex or any of its individual proteins is limited to that inferred from biochemical experiments [16,18,20,24]. Similarly, data regarding the positional knowledge of these shelterin components and how they are organized in a complex is not clear. To begin to fill this knowledge gap, we have used negative-stain electron microscopy (EM) to determine the structural organization of the *S. pombe* CTP complex. Our three-dimensional reconstruction shows that the CTP complex assembles as a dimer of Ccq1-Tpz1-Poz1 heterotrimers. Furthermore, we have employed genetic density labels to identify individual regions of protein subunits within the complex. The structural data is complemented with cross-linking mass spectrometry analyses, which report the proximity of individual proteins at specific residues on or near the interaction interfaces. Together, our data provide the first glimpse into the architecture of the CTP complex and offer useful insight for further understanding the molecular interactions of the shelterin complex that contribute to proper telomere length homeostasis.

The three-dimensional structure of the CTP complex

To gain insight into the molecular topology of the fission yeast Ccq1-Tpz1-Poz1 complex, the individual proteins were expressed or co-expressed in bacteria and the multi-protein assembly was purified to homogeneity. This complex consists of the full-length Ccq1 (C_f) and Poz1 proteins, along with the Tpz1 CTD (406–508) that is both necessary and sufficient for CTP complex formation [16,19]. After purification, the complex (C_fTP) was stabilized by chemical cross-linking using DSSO (disuccinimidyl sulfoxide) [24]. Previous data indicates that co-expression of either Poz1-Tpz1 or Ccq1-Tpz1 results in complexes with molecular masses that are indicative of dimers of heterodimers [24]. Analogously, size-exclusion chromatography of the native C_fTP complex, as well as SDS-PAGE analysis of the cross-linked sample, revealed that the complex has a molecular mass that is indicative of a dimer of heterotrimers (Fig. 2a and b). All together, these results suggest that Tpz1 mediates

coordinated interactions with Poz1 and Ccq1 to assemble a CTP complex that is composed of two copies each of the Ccq1, Tpz1, and Poz1 proteins.

To gain further insight into the molecular architecture of the CTP complex, we determined its structure using electron microscopy and single-particle reconstruction techniques. Micrographs were obtained and individual particles were isolated to generate two-dimensional class averages (Fig 2c). An initial three-dimensional volume of the complex was determined using random-conical-tilt (RCT) procedures [25] (Fig. S2) and analysis of the observed orientations revealed that the particle distribution represents most angular views in three-dimensional space (Fig. 2d). The CTP complex volume was then refined and resolved to a resolution of 34 Å (Fig. S3) to reveal a cage-like conformation with a central cavity and four distinct openings (Fig. 2e). The approximate dimensions of the structure are 123 × 73 × 90Å. Although symmetry operations were not imposed in the reconstruction procedures, the structure revealed a potential mirror-plane of symmetry further supporting the notion that the complex assembles from two heterotrimers. On the front of the assembly, three separate lobes of density were assigned the names L1, L2 and L3. All three lobes coalesced on the backside of the complex to form a triskelion (T) of density (Fig. 2e).

The CTD of Ccq1 homodimerizes in the CTP complex

The relatively low resolution of the EM structure, combined with an absence of any atomic-resolution structures of Ccq1, Poz1, or Tpz1 to dock into the EM volume, posed limitations for interpretation of the map and particularly for the localization of individual proteins within the C_fTP complex. Therefore, another complex was expressed and assembled that lacked the CTDs of Ccq1 (Fig. S4a). A comparison of this structure (Ccq1-NTD, Tpz1, Poz1: C_nTP) with the C_fTP structure was expected to identify missing densities that could be attributed to Ccq1 CTDs. The assembled C_nTP complex revealed a molecular weight that is consistent with that of a complex assembled from two copies each of Ccq1-NTD, Poz1, and Tpz1 (Fig. S4b). These data suggest that the CTD of Ccq1 is not a requirement for CTP complex assembly.

The C_nTP complex was solved using EM and the resulting volume was aligned with the C_fTP complex to identify differences that could be assigned to density of the missing CTDs of Ccq1 in the C_nTP volume. The primary difference between the two maps (C_fTP vs. C_nTP) was identified as the triskelion (T) density formed in the C_fTP complex, which was no longer present in the C_nTP complex (Fig. 3a & S4c and d). Also, while the densities that comprise the L1 and L3 lobes were similar in the two structures, the density comprising the L2 lobe in the C_fTP complex is separated and rearranged in the C_nTP complex. Based on these data, we posited that two Ccq1 CTDs merge to form an interaction that can be attributed to the triskelion density in the C_fTP structure. The loss of the Ccq1-CTD interaction would thereby disrupt a physical link between the two Ccq1 proteins, allowing the individual NTDs to be less constrained and adopt different orientations in the C_nTP complex. To test this hypothesis, we biochemically probed the capability of the individual Ccq1 domains to homodimerize. To this end, Ccq1-CTD eluted off of a size-exclusion column at a size expected for that of a dimer; a finding that was further supported by DSSO

cross-linking and SDS-PAGE analysis (Fig. S4e). In contrast, analysis of the Ccq1-NTD shows that it behaves as a monomer, even in the presence of DSSO cross-linker (Fig. S4e).

Localization of the Ccq1 N-terminal domains

To localize the Ccq1 N-terminal domains (NTD)s in the EM structure, we genetically engineered a maltose-binding protein (MBP)-Ccq1 fusion protein (Fig. S5a) to include in complex assembly (MBP-Ccq1, Tpz1, Poz1 complex: $_{m}C_{f}TP$). The $_{m}C_{f}TP$ complex was purified to homogeneity and stabilized by DSSO cross-linking (Fig. S5b). The mass of MBP was then used as a density label in the EM reconstruction for localization of the Ccq1-NTDs. The structure revealed that the overall shape of the $_{m}C_{f}TP$ complex was similar to that of the $C_{f}TP$ complex, although subtle differences in conformation were observed, most likely due to the insertion of the large MBP tags (Fig. 3b and Fig. S5b). Difference mapping identified two prominent regions of density protruding from the $_{m}C_{f}TP$ complex, which were provisionally assigned to the MBP insertions (Fig. 3b; Supplemental Movie 1). These two regions localized to opposite sides of the CTP complex, where one is between L1 and L2 and the other resides between L2 and L3.

Localization of the Poz1 N-termini

We next used the MBP-density tag to identify the N-termini of Poz1 proteins in the EM structure (Fig. S5). When MBP was expressed on the N-terminus of Poz1, the complex revealed additional densities in the regions of L1 and L3 (Fig. 3c & S5d). Although Ccq1 cannot interact with Poz1 in the absence of Tpz1 [19], our data suggest that Poz1 and Ccq1-NTD are adjacent to one another within the CTP complex. Specifically, our data indicate that Poz1 proteins comprise the L1 and L3 densities within the structure, while Ccq1-NTDs comprise density that connects L1 and L3 with L2. Attempts to construct a CTP complex containing the MBP-Tpz1-CTD fusion protein were unsuccessful, because the MBP on Tpz1 protein interfered with CTP complex assembly. However, because the Tpz1-CTD used in our experiments contains two regions that are essential for its interaction with Ccq1 and Poz1, respectively [16,18,24], we predict that two Tpz1-CTD molecules localize to the juncture connecting Poz1 and Ccq1 proteins. All together these data allowed us to tentatively map the location of each protein/domain within the assembled CTP complex (Fig. 3d).

MICro-MS details the Poz1-Ccq1 physical contact and dimerization of Ccq1-CTD

We next sought to pinpoint the precise contact sites of the inter-subunit interactions within the CTP assembly. To do so, we subjected the CTP complex to a recently developed DSSO based cross-linking mass spectrometry strategy called MICro-MS (Mapping Interfaces via Crosslinking-Mass Spectrometry) [24]. We subjected the purified $Ccq1^{Full}$-$Tpz1^{406–508}$-$Poz1^{Full}$ complex to chemical crosslinking using an optimized concentration of DSSO at 5 mM. As shown in Figure 2b, the crosslinked $Ccq1^{Full}$-$Tpz1^{406–508}$-$Poz1^{Full}$ complex revealed a molecular mass of ~266 kDa, which supports assembly of a dimer of heterotrimers. Similar results were observed using gel filtration to purify the complex in its

native, non-crosslinked form (Fig. 2a). The tryptic digests of crosslinked CTP complexes were analyzed using multistage tandem mass spectrometry (MS^n) (Fig. 4). Representative MS^n spectra for unambiguous identification of DSSO crosslinked peptides are displayed for Ccq1-Poz1 interactions in Figure 4a–c and Figure S5, and for Ccq1-CTD dimerization in Figure 4d–f.

Extensive cross-links were identified between Ccq1-NTD and Poz1, including Ccq1:K146–Poz1:K123, Ccq1:K146–Poz1:K192, Ccq1:K72–Poz1:K192, Ccq1:K72–Poz1:K213, and Ccq1:K78–Poz1:K213, (Fig. 4a–c; Fig. S6). These results reveal a physical interaction between Ccq1 and Poz1 proteins, which likely occurs in the L1 and L3 regions of the CTP EM structure. Additionally, extensive inter- but not intra-molecular cross-links containing overlapping sequences between separate Ccq1-CTDs were detected, which include K578–K584, K578–K589, K589–K597, K597–K635, K598–K635, K605–K635, K632–K641, and K676–K684 (Fig. 4d–f; Fig. S6). These data support the notion that the Ccq1-CTDs come into close proximity of one another, as a homodimer, to form the triskelion density visualized in the EM structure. Finally, crosslinked peptides between Tpz1 and Ccq1, as well as those between Tpz1 and Poz1 were identified in the DSSO-crosslinked CTP complex. These data were similar to those previously identified in the context of Tpz1-Ccq1 and Tpz1-Poz1 binary complexes reported previously [24]. In summary, the MICro-MS results identified several unique pairs of residues that are near the Ccq1-Poz1 interface and others that support the homodimerization of Ccq1-CTDs (Fig. 4g).

Discussion

The dimerization of telomere end-binding proteins has long been implicated as an important process in regulating telomere length homeostasis. For example, Cdc13 homodimerization events regulate telomere length in *S. cerevisiae* by forming optimal binding sites for the catalytic subunit of DNA polymerase α and for Stn1 [26,27]. In mammals, phosphorylation of ACD governs its homodimerization to regulate the concentrations of POT1 and ACD accumulating at telomeres [28]. The double-stranded DNA-binding proteins, including TRF1 and TRF2 in mammals and Taz1 in fission yeast, predominantly bind telomere DNA as preformed homodimers to maintain proper telomere length [29,30]. Mutations that abrogate *S. pombe* Taz1 dimerization result in a 10-fold decrease in telomeric DNA-binding *in vitro* and fail to associate with telomeres *in vivo* [31]. As a result, the dimerization-deficient *taz1* mutant cells bear heterogeneously elongated telomeres, similar to those in *taz1*Δ cells, thereby punctuating the critical role of Taz1 dimerization in regulating telomere length. Similarly, fission yeast Rap1 forms a homodimer and interacts with Taz1 directly in the context of the telomere shelterin complex [32]. In consideration of these data, and in light of our finding that the CTP complex is dimeric, it can be surmised that the dimerization of the shelterin complex regulates telomere protection and synthesis, perhaps by specifically facilitating the cooperative binding of shelterin to sister chromatids so that both telomeres can be effectively protected and/or simultaneously extended by telomerase.

With the use of MBP-tagging as a labeling strategy, as well as the exclusion of the CTDs of Ccq1 from the complex, we were able to tentatively map the Ccq1 C-termini to the triskelion density of the cage-like structure, the Ccq1 NTDs to the L1 and L3 lobes, and the Poz1

proteins immediately adjacent to the L1 and L3 lobes. We have identified intermolecular interactions within the CTDs of Ccq1 proteins that support the role of this domain in facilitating homodimerization. However, assembly of the CTP complex involves additional interactions. This observation becomes apparent in our C_nTP structure, which demonstrates that the CTP dimer is maintained even in the absence of the Ccq1 CTDs. Taken together, these observations support a scenario in which the CTP dimer is stabilized by multiple intermolecular interactions that exist between all three proteins within the CTP complex.

Molecular interactions between the Tpz1 CTD and the Ccq1 NTD, as well as those between the Tpz1 CTD and Poz1 protein, have been characterized independently [16,19]. Therefore, the most plausible location for Tpz1 is at the Ccq1-Poz1 juncture, where it interacts with both proteins [18]. Interestingly, a contact interface is indicated between Ccq1 and Poz1 in our EM structure, and is independently supported by extensive cross-links identified between the two proteins. In the absence of Tpz1, however, yeast two-hybrid assays failed to detect any direct interaction between Ccq1 and Poz1 [18,19]. These data further support the placement of Tpz1 at the Ccq1-Poz1 interface where it is ideally positioned to coordinate its functional role in regulating interactions to positively or negatively regulate telomerase-mediated telomere elongation.

Specifically, as a sub-complex of shelterin, the CTP complex contains the interface between the positive regulator (Ccq1) and negative regulator (Poz1) of telomerase-mediated telomere elongation. This interface is a critical regulatory center in determining whether a telomere would be in an extendible or non-extendible state. Indeed, while the mechanism is not well understood, the Tpz1-Ccq1 and Tpz1-Poz1 interactions are important in regulating Ccq1-T93 phosphorylation in a positive and a negative way, respectively [18,21]. Based on the proximity of Ccq1 NTD with the Poz1 protein, it is possible that Poz1 sterically hinders the Ccq1-T93 phosphorylation site from being accessible to $Rad3^{ATR}/Tel1^{ATM}$ kinases. At the same time, the compact structure of the CTP complex establishes a structural basis for simultaneously exposing a coupled telomere-telomerase contact point, namely the Ccq1-Est1 and Tpz1-Trt1 interfaces, to better facilitate telomerase recruitment to the CTP complex. Similarly, phosphorylation of ACD, also during S phase, is an event that has been reported to increase the stability of telomere-telomerase interactions in mammals [33]. These data point to a generally conserved mechanism, at least between mammals and fission yeast, where telomere-telomerase interactions are regulated by post-translational modification to control telomere length homeostasis.

Our combined EM-MS investigations establish the most comprehensive structural model of the CTP complex currently available. Furthermore, our results provide an expanded guide to address the protein arrangement and protein-protein interactions of the CTP complex at the telomere. Therefore, our structural model provides an important foundation for additional and more detailed structure-function relationship and mechanistic studies related to shelterin integrity and telomerase-mediated interactions.

Supplementary Material

Refer to Web version on PubMed Central for supplementary material.

Acknowledgments

We thank Heather Holdaway and Sudheer Molugu for technical expertise and for managing the electron microscopes. This work was supported by grants from the NIH (DP2 CA186571 to D.J.T., R01 GM098943 to F.Q., R01GM074830 and R01GM106003 to L.H.) and the American Cancer Society (RSG-13-211-01-DMC to D.J.T. and RSG-16-041-01-DMC to F.Q.).

Abbreviations used

ssDNA	single-stranded deoxyribonucleic acid
dsDNA	double-stranded deoxyribonucleic acid
RNP	ribonucleoprotein
MBP	Maltose Binding Protein
TRF1	telomeric repeat-binding factor 1
TRF2	telomeric repeat-binding factor 2
POT1	protection of telomeres protein 1
ACD	adrenocortical dysplasia
TIN2	TRF1-interacting nuclear factor 2
CLRC	Clr4 methyltransferase complex
CTD	C-terminal domain
NTD	N-terminal domain
Ccq1	Coiled-coil quantitatively-enriched protein 1
Tpz1	protection of telomeres protein Tpz1
Poz1	protection of telomeres Poz1
Taz1	telomere length regulator Taz1
Est1	telomere elongation protein Est1
Rad3	DNA repair helicase Rad3
Tel1	serine/threonine protein kinase Tel1
Ccd13	cell-division control protein 13
Stn1	CST complex subunit Stn1
RCT	random conical tilt
EM	electron microscopy
DSSO	disuccinimidyl sulfoxide

References

1. Nandakumar J, Cech TR. Finding the end: recruitment of telomerase to telomeres. Nat Rev Mol Cell Biol. 2013; 14:69–82. DOI: 10.1038/nrm3505 [PubMed: 23299958]
2. Huffman KE, Levene SD, Tesmer VM, Shay JW, Wright WE. Telomere Shortening Is Proportional to the Size of the G-rich Telomeric 3′-Overhang *. 2000; 275:19719–19722. DOI: 10.1074/jbc.M002843200
3. Blackburn EH, Greider CW, Szostak JW. Telomeres and telomerase: the path from maize, Tetrahymena and yeast to human cancer and aging. Nat Med. 2006; 12:1133–1138. DOI: 10.1038/nm1006-1133 [PubMed: 17024208]
4. Harley CB, Futcher AB, Greider CW. Telomeres shorten during ageing of human fibroblasts. Nature. 1990; 345:458–60. DOI: 10.1038/345458a0 [PubMed: 2342578]
5. Denchi EL, de Lange T. Protection of telomeres through independent control of ATM and ATR by TRF2 and POT1. Nature. 2007; 448:1068–71. DOI: 10.1038/nature06065 [PubMed: 17687332]
6. Sfeir T, Agnel J, de Lange. Removal of Shelterin Revelas the Telomere End-Replication Problem. Science (80-). 2012; 336:593–597. DOI: 10.1126/science.1218498.Removal
7. Guo X, Deng Y, Lin Y, Cosme-Blanco W, Chan S, He H, Yuan G, Brown EJ, Chang S. Dysfunctional telomeres activate an ATM-ATR-dependent DNA damage response to suppress tumorigenesis. EMBO J. 2007; 26:4709–4719. DOI: 10.1038/sj.emboj.7601893 [PubMed: 17948054]
8. Hastie ND, Dempster M, Dunlop MG, Thompson AM, Green DK, Allshire RC. Telomere reduction in human colorectal carcinoma and with ageing. Nature. 1990; 346:866–868. DOI: 10.1038/346866a0 [PubMed: 2392154]
9. de Lange T. How telomeres solve the end-protection problem. Science (80-). 2009; 326:948–52. DOI: 10.1126/science.1170633
10. Verdun RE, Karlseder J. Replication and protection of telomeres. Nature. 2007; 447:924–931. DOI: 10.1038/nature05976 [PubMed: 17581575]
11. Greider CW, Blackburn EH. A telomeric sequence in the RNA of Tetrahymena telomerase required for telomere repeat synthesis. Nature. 1989; 337:331–7. DOI: 10.1038/337331a0 [PubMed: 2463488]
12. Nakamura TM, Morin GB, Chapman KB, Weinrich SL, Andrews WH, Lingner J, Harley CB, Cech TR. Telomerase catalytic subunit homologs from fission yeast and human. Science. 1997; 277:955–9. DOI: 10.1126/science.277.5328.955 [PubMed: 9252327]
13. De Lange T. Shelterin: The protein complex that shapes and safeguards human telomeres. Genes Dev. 2005; 19:2100–2110. DOI: 10.1101/gad.1346005 [PubMed: 16166375]
14. Rajavel M, Mullins MR, Taylor DJ. Multiple facets of TPP1 in telomere maintenance. Biochim Biophys Acta. 2014; 1844:1550–9. DOI: 10.1016/j.bbapap.2014.04.014 [PubMed: 24780581]
15. Takai KK, Kibe T, Donigian JR, Frescas D, De Lange T. Article Telomere Protection by TPP1/POT1 Requires Tethering to TIN2. Mol Cell. 2011; 44:647–659. DOI: 10.1016/j.molcel.2011.08.043 [PubMed: 22099311]
16. Jun HI, Liu J, Jeong H, Kim JK, Qiao F. Tpz1 controls a telomerase-nonextendible telomeric state and coordinates switching to an extendible state via Ccq1. Genes Dev. 2013; 27:1917–1931. DOI: 10.1101/gad.219485.113 [PubMed: 24013504]
17. Wang J, Cohen AL, Letian A, Tadeo X, Moresco JJ, Liu J, Yates JR, Qiao F, Jia S. The proper connection between shelterin components is required for telomeric heterochromatin assembly. Genes Dev. 2016; 30:827–839. DOI: 10.1101/gad.266718.115 [PubMed: 26988418]
18. Harland JL, Chang YT, Moser BA, Nakamura TM. Tpz1-Ccq1 and Tpz1-Poz1 Interactions within Fission Yeast Shelterin Modulate Ccq1 Thr93 Phosphorylation and Telomerase Recruitment. PLoS Genet. 2014; 10doi: 10.1371/journal.pgen.1004708
19. Miyoshi T, Kanoh J, Saito M, Ishikawa F. Fission Yeast Pot1-Tpp1 Protects Telomeres and Regulates Telomere Length. Science (80-). 2008; 320:1341–1344. DOI: 10.1126/science.1154819

20. Moser BA, Chang YT, Kosti J, Nakamura TM. Tel1ATM and Rad3ATR kinases promote Ccq1-Est1 interaction to maintain telomeres in fission yeast. Nat Struct Mol Biol. 2011; 18:1408–13. DOI: 10.1038/nsmb.2187 [PubMed: 22101932]
21. Yamazaki H, Tarumoto Y, Ishikawa F. Tel1ATM and Rad3ATR phosphorylate the telomere protein Ccq1 to recruit telomerase and elongate telomeres in fission yeast. Genes Dev. 2012; 26:241–246. DOI: 10.1101/gad.177873.111 [PubMed: 22302936]
22. Hu X, Liu J, Jun HI, Kim JK, Qiao F. Multi-step coordination of telomerase recruitment in fission yeast through two coupled telomere-telomerase interfaces. Elife. 2016; 5doi: 10.7554/eLife.15470
23. Chang YT, Moser BA, Nakamura TM. Fission Yeast Shelterin Regulates DNA Polymerases and Rad3ATR Kinase to Limit Telomere Extension. PLoS Genet. 2013; 9doi: 10.1371/journal.pgen.1003936
24. Liu J, Yu C, Hu X, Kim J, Bierma JC, Jun H, Rychnovsky SD, Huang L, Qiao F. Dissecting Fission Yeast Shelterin Interactions via MICro-MS Links Disruption of Shelterin Bridge to Tumorigenesis. Cell Rep. 2015; 12:2169–2180. DOI: 10.1016/j.celrep.2015.08.043 [PubMed: 26365187]
25. Radermacher M, Wagenknecht T, Verschoor A, Frank J. Three-dimensional reconstruction from a single-exposure, random conical tilt series applied to the 50S ribosomal subunit of Escherichia coli. J Microsc. 1987; 146:113–136. DOI: 10.1111/j.1365-2818.1987.tb01333.x [PubMed: 3302267]
26. Sun J, Yang Y, Wan K, Mao N, Yu TY, Lin YC, DeZwaan DC, Freeman BC, Lin JJ, Lue NF, Lei M. Structural bases of dimerization of yeast telomere protein Cdc13 and its interaction with the catalytic subunit of DNA polymerase α. Cell Res. 2011; 21:258–74. DOI: 10.1038/cr.2010.138 [PubMed: 20877309]
27. Mason M, Wanat JJ, Harper S, Schultz DC, Speicher DW, Johnson FB, Skordalakes E. Cdc13 OB2 dimerization required for productive stn1 binding and efficient telomere maintenance. Structure. 2013; 21:109–120. DOI: 10.1016/j.str.2012.10.012 [PubMed: 23177925]
28. Han X, Liu D, Zhang Y, Li Y, Lu W, Chen J, Songyang Z. Akt Regulates TPP1 Homodimerization and Telomere Protection. Aging Cell. 2013; 12:1091–1099. DOI: 10.1111/acel.12137 [PubMed: 23862686]
29. Bianchi A, Stansel RM, Fairall L, Griffith JD, Rhodes D, De Lange T. TRF1 binds a bipartite telomeric site with extreme spatial flexibility. EMBO J. 1999; 18:5735–5744. DOI: 10.1093/emboj/18.20.5735 [PubMed: 10523316]
30. Spink KG, Evans RJ, Chambers a. Sequence-specific binding of Taz1p dimers to fission yeast telomeric DNA. Nucleic Acids Res. 2000; 28:527–533. gkd160 [pii]. [PubMed: 10606652]
31. Deng W, Wu J, Wang F, Kanoh J, Dehe P-M, Inoue H, Chen J, Lei M. Fission yeast telomere-binding protein Taz1 is a functional but not a structural counterpart of human TRF1 and TRF2. Cell Res. 2015; :1–4. DOI: 10.1038/cr.2015.76
32. Chikashige Y, Hiraoka Y. Telomere binding of the Rap1 protein is required for meiosis in fission yeast. Curr Biol. 2001; 11:1618–1623. DOI: 10.1016/S0960-9822(01)00457-2 [PubMed: 11676924]
33. Zhang Y, Chen L-Y, Han X, Xie W, Kim H, Yang D, Liu D, Songyang Z, Mclean M, Thomas Cech R. Phosphorylation of TPP1 regulates cell cycle-dependent telomerase recruitment. n.d; doi: 10.1073/pnas.1217733110
34. Tang G, Peng L, Baldwin PR, Mann DS, Jiang W, Rees I, Ludtke SJ. EMAN2: An extensible image processing suite for electron microscopy. J Struct Biol. 2007; 157:38–46. DOI: 10.1016/j.jsb.2006.05.009 [PubMed: 16859925]
35. Scheres SHW. RELION: Implementation of a Bayesian approach to cryo-EM structure determination. J Struct Biol. 2012; 180:519–530. DOI: 10.1016/j.jsb.2012.09.006 [PubMed: 23000701]
36. Mindell JA, Grigorieff N. Accurate determination of local defocus and specimen tilt in electron microscopy. J Struct Biol. 2003; 142:334–347. DOI: 10.1016/S1047-8477(03)00069-8 [PubMed: 12781660]
37. Kao A, Chiu C, Vellucci D, Yang Y, Patel VR, Guan S, Randall A, Baldi P, Rychnovsky SD, Huang L. Development of a novel cross-linking strategy for fast and accurate identification of

cross-linked peptides of protein complexes. Mol Cell Proteomics. 2011; 10:M110.002212.doi: 10.1074/mcp.M110.002212

Highlights

- The CTP complex coordinates telomere extension and protection in *S. pombe*
- The CTP complex is a dimer of trimers
- 34Å resolution model of the CTP complex, solved by negative-stain EM
- CTP subunit locations described
- MICro-MS identifies unique interactions between Ccq1-Poz1 and supports Ccq1 CTD dimerization

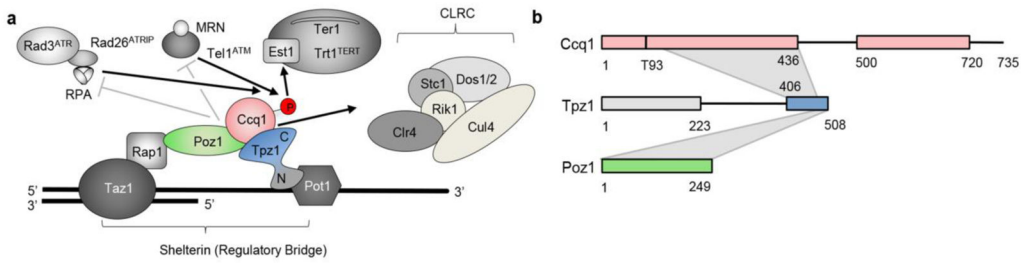

Figure 1.

Schematic representation depicting the diverse roles of the CTP complex in telomere homeostasis. (a) The intact shelterin complex interconnects telomeric ssDNA and dsDNA to regulate different cellular pathways. Destabilization of CTP interactions affects Rad3/Tel1 dependent phosphorylation of Ccq1 Thr93, which directs telomerase recruitment and telomere extension. Similarly, Ccq1-Tpz1 interactions are important for the recruitment of the CLRC complex and silencing of nearby marker genes. (b) Cartoon diagram depicting the interactions between the individual proteins that comprise the CTP complex.

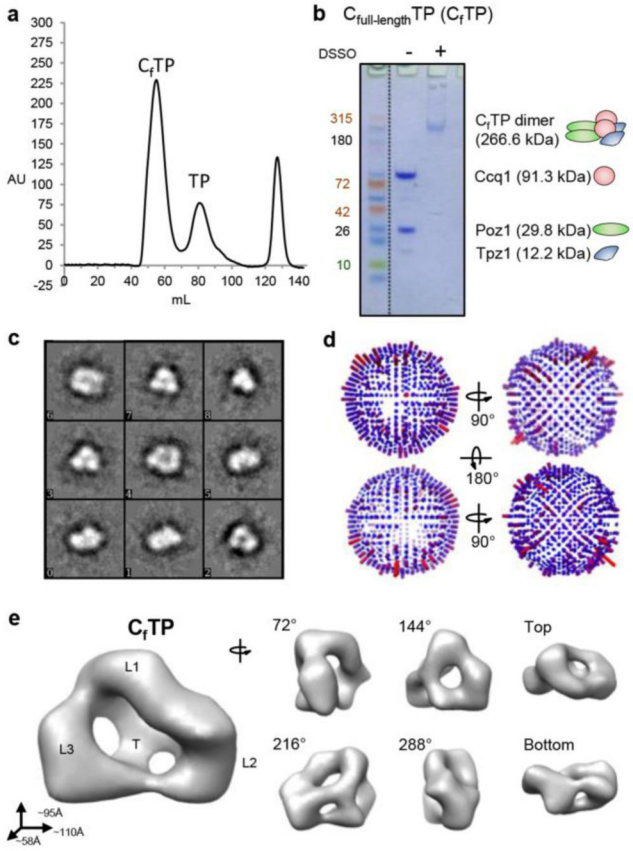

Figure 2.

The three-dimensional structure of the CTP complex reveals a cage-like complex assembled as a dimer of heterotrimers. (a) Size-exclusion profile of the assembled C_fTP complex. (b) SDS-PAGE analysis of the C_fTP with and without DSSO cross-linker. (c) Representative two-dimensional class averages of the C_fTP complex generated from electron microscopy images. (d) Angular distribution of the electron microscopy projections of the C_fTP complex that contributed to the three-dimensional reconstruction. (e) Surface rendering of the three-dimensional structure of the C_fTP complex filtered to 34 Å resolution. Labels identify areas of density described as triskelion (T) and L1, L2, and L3 lobes. The panel includes different views of the structure at the defined angles of rotation. For bacterial expression of *S. pombe* proteins, cDNA for Ccq1-NTD (2–439), Ccq1-CTD (504–719); Ccq1 (2–716; full-length), and Poz1 (2–249)/Tpz1(406–508) were cloned into a modified pET28-6His-SUMO vector with Ulp1-cleavage site following the 6His-SUMO tag (Champion™ pET SUMO protein expression system, Invitrogen, CA) and subsequently transformed into Rosetta-BL21 (DE3) cells. Protein expression was induced with 0.4 mM isopropyl-β-$_D$-1-thiogalactopyranoside (IPTG) for 5 hr at 30°C. The complex was purified with affinity purification using the 6His-tag followed by anion exchange on a HiTrap Q column. To stabilize complexes for EM imaging, C_fTP was chemically cross-linked using 10 mM DSSO for 1 hr on ice before quenching with 2μl 1 M Tris-HCl pH 8.0 for 15 min. The cross-linked complexes were further purified on a G200 10/300GL column (GE Healthcare). EM grids were prepared using 3.5 μL of 200 nM purified complex on glow-discharged carbon-coated, copper grids.

The grids were stained in 2% uranyl acetate and data were collected at 200 keV on a FEI TF-20 transmission electron microscope (TEM) at 42.67kX (3.654 Å/pixel) equipped with a 4k × 4k TVIPS CCD camera. After selection of 1006 particle pairs in EMAN2.0 [34], particles were CTF-corrected and subjected to reference-free alignment to produce class averages and to generate an initial model using random conical tilt procedures. Particles were imported into RELION 1.3 [35] for further 3D refinement.

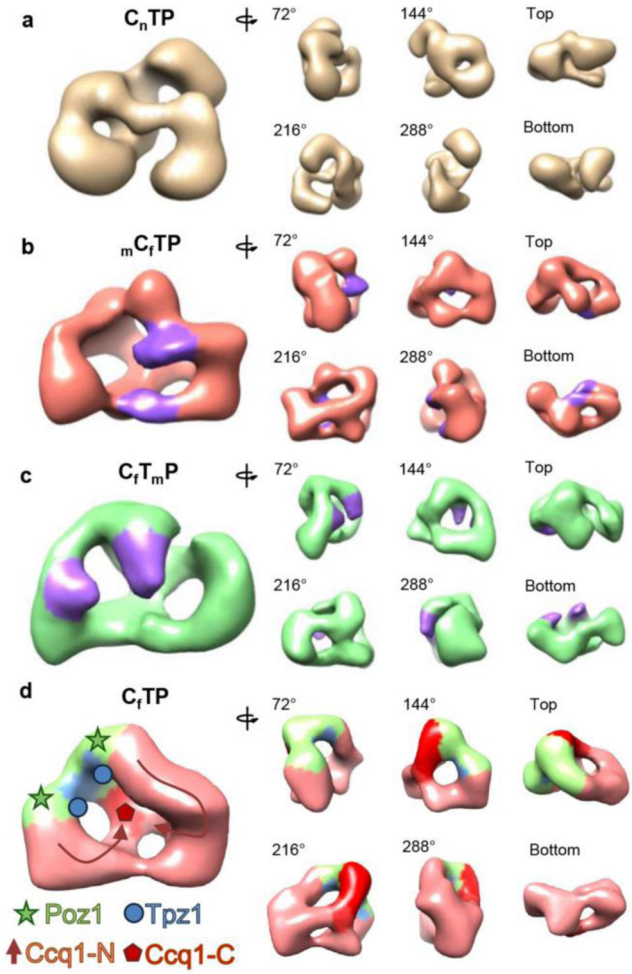

Figure 3.

Localization of the individual protein subunits in the CTP complex. (a) The C_nTP structure indicates that the missing Ccq1 C-terminal domains were responsible for forming the triskelion density in the C_fTP complex. The volume is rotated at different angles as defined. The C_nTP complex was purified in a similar manner as the C_fTP complex. (b) The $_mC_fTP$ structure reveals two masses of density that can be attributed to the MBP tags (colored purple) in the 3D reconstruction. The MBP densities identify the proximity of the Ccq1 N-termini. The various angular views on the right side of the panel are at the same angles as those defined in panel a. (c) The C_fT_mP structure reveals two masses of density that can be attributed to the MBP tags (colored purple) in the 3D reconstruction. The MBP densities identify the proximity of the Poz1 N-termini. (d) Subunit assignments based on MBP tagging and biochemical data. The various angular views on the right side of the panel are at the same angles as those defined in panel a. For MBP-fusion proteins, Ccq1 or Poz1(2–249)/Tpz1(406–508) constructs were cloned into a modified pET vector with an MBP tag residing at the N-terminus of the target protein construct. The expression, purification, cross-linking, grid preparation, and data collection were the same as described for C_fTP. Micrographs were imported into RELION1.3 and subjected to CTF estimation using

CTFFIND3 [36]. Approximately 1000 particles were manually selected and subjected to reference-free alignment to generate class averages that were used as templates for autopicking procedures, which were subjected to reference-free alignment to produce class averages and for three-dimensional classification using the C_fTP model as a reference. The three-dimensional volumes were generated using projection alignment procedures and CTF correction, followed by multiple rounds of angular refinement.

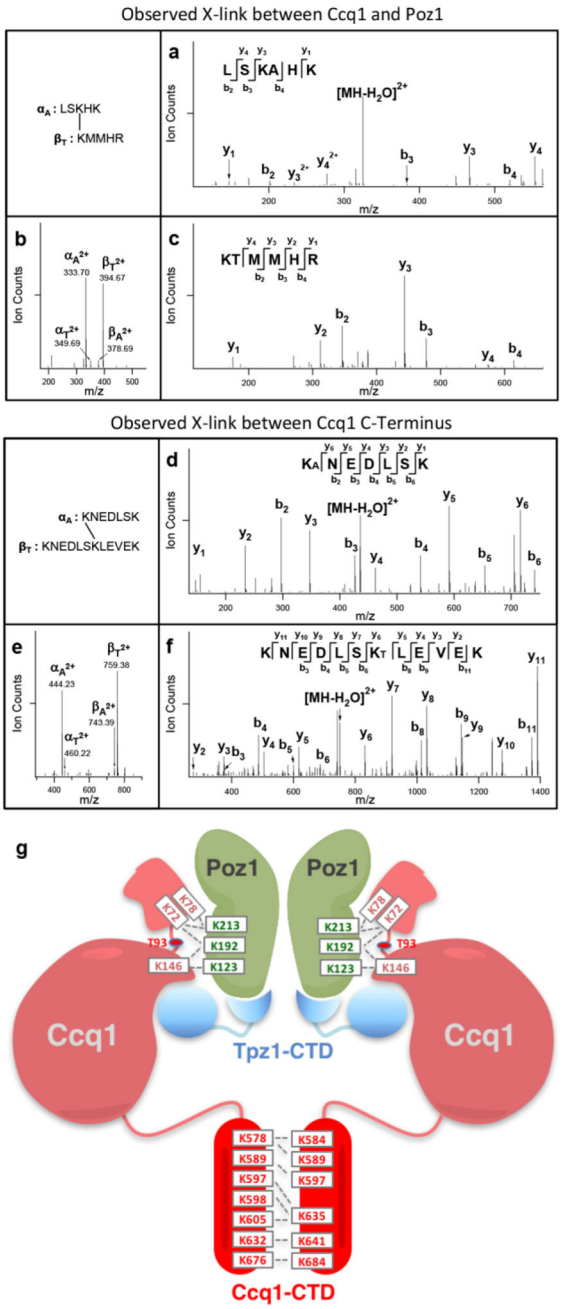

Figure 4.

MS^n analysis of an inter-subunit DSSO cross-link between Ccq1 and Poz1 peptides. (a) MS^2 spectrum of DSSO inter-linked Ccq1 peptides α-β (*m/z* 606.3066^{4+}) yielding characteristic fragment ion pairs α_A/β_T (*m/z* $444.23^{2+}/759.38^{2+}$) and α_T/β_A (*m/z* $460.22^{2+}/743.39^{2+}$). (b) MS^3 spectrum of fragment α_A (*m/z* 444.23^{2+}), resulting in the detection of series of b (b_2~b_6) and y (y_1~y_6) ions unambiguously identifying α as ^{578}KNEDLSK^{584} of Ccq1. (c) MS^3 spectrum of fragment β_T (*m/z* 759.38^{2+}), which yielded series of b (b_3~b_6, b_8, b_9, b_{11}) and y (y_2~y_{11}) ions unambiguously identifying β as ^{578}KNEDLSKLEVEK^{589} of Ccq1. Overlap of peptide sequences in α and β indicate that this cross-link describes a covalent

linkage between two different Ccq1 proteins. (d) MS^2 spectrum of DSSO inter-linked Ccq1 and Poz1 peptides α-β (*m/z* 368.6900^{4+}) yielding characteristic fragment ion pairs α_A/β_T (*m/z* $333.70^{2+}/394.67^{2+}$) and α_T/β_A (*m/z* $349.69^{2+}/378.69^{2+}$). (e) MS^3 spectrum of fragment α_A (*m/z* 333.70^{2+}), resulting in the detection of series of b (b_2~b_4) and y (y_1, y_3, y_4) ions unambiguously identifying α as ^{188}LSKHK^{192} of Poz1. (f) MS^3 spectrum of fragment β_T (*m/z* 394.67^{2+}), which yielded series of b (b_2~b_4) and y (y_1~y_4) ions unambiguously identifying β as ^{146}KMMHR^{150} of Ccq1. (g) Schematic representation summarizing the cross-link pairs identified within the CTP complex. The MS analysis was performed with 45 μl purified Ccq1(2–716)/Tpz1(406–508)/Poz1(2–249) complex (4.5 mg/ml) which was mixed with 5 μl 100 mM DSSO in DMSO to the final concentration of 10 mM. Cross-linking was performed for 30 min on ice and quenched with 2 μl 1M Tris-HCl (pH8.0) for 15 min. The cysteine residues were reduced with 4 mM TCEP and alkylated with 20 mM iodoacetamide in dark, followed by terminating alkylation reaction with 20 mM cysteine for 30 min. The cross-linked proteins were digested overnight at 37 °C with trypsin (2% w/w) and chymotrypsin (5% w/w), separately. Cross-linked peptides were analyzed by LC MS^n utilizing an LTQ-Orbitrap XL MS (Thermo Fisher, San Jose, CA) coupled on-line with an Easy-nLC 1000 (Thermo Fisher, San Jose, CA) as previously described [37]. Each MS^n experiment consists of one MS scan in FT mode (350–1400 m/z, resolution of 60,000 at m/z 400) followed by two data-dependent MS^2 scans in FT mode (resolution of 7500) with normalized collision energy at 20% on the top two MS peaks with charges 3^+ or up, and three MS^3 scans in the LTQ with normalized collision energy at 35% on the top three peaks from each MS^2.